

1  
2  
3  
4  
5  
6  
7  
8  
9  
10  
11  
12  
13  
14  
15  
16  
17  
18  
19

# **STAR-ESDM: A Generalizable Approach to Generating High-Resolution Climate Projections through Signal Decomposition**

**Katharine Hayhoe<sup>1,2</sup>, Ian Scott-Fleming<sup>1</sup>, Anne Stoner<sup>3</sup> and Donald J. Wuebbles<sup>3,4</sup>**

<sup>1</sup> Climate Center, Texas Tech University, Lubbock TX 79409 USA.

<sup>2</sup> The Nature Conservancy, 4245 Fairfax Dr., Arlington VA 22203 USA.

<sup>3</sup> Earth Knowledge, Inc., Tucson AZ 85751 USA.

<sup>4</sup> Dept. of Atmospheric Sciences, University of Illinois at Urbana-Champaign, Urbana IL 61801 USA.

Corresponding author: Katharine Hayhoe ([katharine.hayhoe@ttu.edu](mailto:katharine.hayhoe@ttu.edu))

## **Key Points:**

- We've developed a rapid, flexible and generalizable approach to bias-correct & downscale climate model output to any observational dataset
- Model stationarity ensures projected changes in temperature and precipitation are similar to those generated by a high-resolution global model
- STAR-ESDM can be applied using predictors/predictands from global/regional climate models, satellites, reanalysis, and weather stations.

## 20 **Abstract**

21 High-resolution climate projections provide crucial insights into assessing climate risk and  
22 developing climate resilience strategies. The Seasonal Trends and Analysis of Residuals  
23 empirical statistical downscaling model (STAR-ESDM) is a computationally-efficient and  
24 flexible approach to generating high-resolution climate projections that can be applied globally  
25 using a broad range of predictands and predictors that can be sourced from weather stations,  
26 gridded datasets, satellites, reanalysis, and global or regional climate models. It uses signal  
27 processing combined with Fourier filtering and kernel density estimation techniques to  
28 decompose and smooth any quasi-Gaussian time series, gridded or point-based, into multi-  
29 decadal long-term means and/or trends; static and dynamic annual cycles; and probability  
30 distributions of high-frequency variability. Long-term predictor trends are bias-corrected and  
31 predictor components are used to map remaining predictand components to future conditions.  
32 Components are then recombined for each station or grid cell to produce a continuous, high-  
33 resolution bias-corrected and downscaled time series at the spatial and temporal scale of the  
34 original time series. Comparing STAR-ESDM output with high-resolution daily temperature and  
35 precipitation projections generated by a fully dynamical global model demonstrates that the  
36 method is extremely robust, capable of accurately reproducing projected changes for all but the  
37 most extreme temperature and precipitation values. For most continental areas, biases in 1-in-  
38 1000 hottest and coldest temperatures are less than 0.5°C and biases in the 1-in-1000 wet day  
39 precipitation amounts are less than 5 mm/day. As climate impacts intensify, STAR-ESDM  
40 represents a significant advance in generating consistent high-resolution projections to  
41 comprehensively assess risk and optimize resilience.

## 42 **Plain Language Summary**

43 The STAR-ESDM tool is able to quickly and accurately generate climate projections for  
44 individual weather stations and high-resolution grids anywhere in the world. It does this by  
45 breaking down global or regional climate model output into different components, from the long-  
46 term trend to the day-to-day variability, then merging modelled projected changes with  
47 observations. When tested against projections generated by a much more computationally  
48 expensive and complex fully dynamical global model, STAR-ESDM produced almost the same  
49 output even for very extreme temperature and precipitation values, at a fraction of the  
50 computational cost. Moreover, unlike most statistical downscaling models, this method isn't tied  
51 to any specific geographic area or predictand and/or predictor dataset. It can be applied to any  
52 regional or global dataset, whether generated by a climate or reanalysis model, derived from  
53 satellite observations, recorded at weather stations, and more. As climate impacts escalate,  
54 STAR-ESDM offers a flexible and effective way to generate the high-resolution climate  
55 projections needed to better gauge climate risk and enhance resilience anywhere in the world  
56 where reliable observational or quasi-observational data, including from reanalysis or satellites,  
57 are available.

## 58 **1 Introduction**

59 Climate is now changing faster than any time in human history due to human activities,  
60 primarily emissions of greenhouse gases (IPCC, 2021a). These changes are already impacting  
61 food production, water quality, and infrastructure (IPCC, 2022) as well as increasing the  
62 frequency and/or intensity of many types of extreme events including heatwaves and heavy  
63 downpours (IPCC, 2021a). Quantifying the risks these rapid changes pose to human society and

64 the natural environment can provide critical input to resilience and adaptation planning while  
65 simultaneously highlighting the need for mitigation. As the impacts of climate change become  
66 increasingly evident around the world, the urgency of such assessments – and the need for  
67 approaches to generating projections that can be applied globally, especially in the most  
68 vulnerable regions which often lack abundant observational data or modeling capacity – is  
69 increasing rapidly.

70 Future projections typically begin with a range of plausible scenarios that describe the  
71 emissions resulting from a consistent set of human choices regarding climate policy, energy, land  
72 use, population and more (Hayhoe et al. 2017; Chen et al. 2021). These projections are then used  
73 as input to global climate models (GCMs) that divide the atmosphere, ocean, and land surface up  
74 into millions of discrete cells to solve numerical equations representing the physical, biological,  
75 and chemical phenomena in each, as well as inter-cell transfer of water, gases, energy, and more.  
76 As output, GCMs generate gridded projections of key variables including temperature,  
77 precipitation, wind direction and speed, humidity, and other variables that characterize the  
78 evolution of long-term climatic conditions as well as shorter-term variability.

79 The horizontal spatial resolution of GCMs has increased significantly over the past few  
80 decades, with grid cells for CMIP6 models typically ranging from approximately 50 to 260 km  
81 per side (IPCC, 2021b). However, most climate resilience and preparedness efforts require  
82 climate inputs at spatial and sometimes temporal scales much finer than the resolution of even  
83 the latest GCMs (Kotamarthi et al. 2021). In addition, both regional and global model output is  
84 often biased relative to observations due to both structural and parametric uncertainty in the  
85 models as well as the unavoidable fact that the average of a grid cell, particularly for temperature  
86 or precipitation extremes over land, is rarely representative of the value at an individual location  
87 or smaller area within the grid cell. Use of regionally homogenous and/or biased output to  
88 calculate the impacts of, for example, extreme heat on the human body, crop yields, or flood risk  
89 due to heavy precipitation, will yield errors that could in turn result in adaptation measures that  
90 are insufficient (if the projections under-estimate future change, creating a Type 2 or false  
91 negative error) or overly expensive and stringent (if projections over-estimate future change, a  
92 Type 1 or false positive error).

93 These challenges are not unique to climate modeling; they are also relevant to the field of  
94 numerical weather modeling, where they were initially addressed by combining model output  
95 with observations to create a series of multivariate regression corrections such as Model Output  
96 Statistics (Glahn & Lowry, 1972). In a similar way, biases can be removed from climate model  
97 output by combining statistical methods with observed data. Specifically, empirical statistical  
98 bias correction and downscaling of climate model projections introduces new information from  
99 observations and combines this information with model output to generate higher-resolution  
100 projections based on coarser-resolution fields consisting of local weather and climate  
101 characteristics like temperature, humidity, and precipitation.

102 The application of statistical methods to bias correcting GCM output was first proposed  
103 by Karl et al. (1990) as “a method, called climatological projection by model statistics, to relate  
104 GCM grid-point free-atmosphere statistics, the predictors, to these important local surface  
105 observations.” Since then, hundreds of ESDMs have been developed and published, each  
106 describing a separate method or additional development of statistical bias correction and  
107 downscaling method. Previously independent methods have been combined and additional  
108 advanced statistical and computational techniques applied, including neural networks, clustering

109 methods such as expectation-maximization algorithms, combined statistical-dynamical  
110 approaches, machine learning techniques, and deep learning models (e.g., Coulibaly et al. 2005;  
111 Vrac et al. 2007a; Walton et al. 2015; Sachindra et al. 2018; Hernanz et al. 2022; Wang & Tian,  
112 2022). This abundance of methods, a number of which we were involved in developing or  
113 evaluating (e.g. Vrac et al., 2007b; Stoner et al., 2012; Barsugli et al. 2013; Dixon et al. 2016),  
114 begs the obvious question: Why is another needed? Why STAR-ESDM?

115 Despite the plethora of statistical methods and the more than 30-year period over which  
116 they have been developed, stakeholders still do not have a tool that fully encompasses all that the  
117 scientific modeling community can provide. With the notable exception of the Statistical  
118 DownScaling Model (SDSM, Wilby et al. 2002), most ESDMs are developed for a specific  
119 geographic region. This has led to a plethora of different ESDMs being applied to generate  
120 projections for watersheds, regions, and countries around the world; differences between those  
121 projections, especially at the tails of the distribution, are difficult to resolve without digging into  
122 the nuances of each model. In addition, the predictors and predictands for most ESDMs are hard-  
123 wired into the model. It can be difficult and time-consuming to update them with new CMIP  
124 simulations or different predictands, and typically that new data must be in the same format as  
125 the original predictor and predictand for which they were designed: gridded or station-based.  
126 Other ESDMs may demonstrate high reliability in simulating important features such as wet and  
127 dry spells, but were designed more as a proof of concept than a tool that can be used by  
128 stakeholders on a regular basis (e.g. Vrac et al. 2007a).

129 As discussed in Kotamarthi et al. (2021), there is a significant and growing demand for  
130 projections that are: (1) robust, with clearly quantifiable accuracy; (2) generalizable and flexible,  
131 applicable to any region of the world and any observational or modelled dataset; (3) capable of  
132 rapidly bias-correcting and downscaling large suites of global or regional climate model output  
133 for multiple scenarios; and (4) can be used with confidence to calculate increasing risks for  
134 applications where absolute values are required, such as extreme heat, changing energy demand,  
135 shifting crop yields, changes in water demand and supply, and more. Many existing methods  
136 meet one or more of these criteria, but few if any meet them all.

137 Our objective in developing STAR-ESDM is to create a highly functional and  
138 generalizable ESDM that addresses these four stakeholder concerns, and that can be applied  
139 broadly around the world using any predictand dataset in which the user has confidence.  
140 Building on previous research (e.g. Hayhoe et al., 2004, 2008; Stoner et al., 2012) and evaluation  
141 techniques (Dixon et al. 2016) we have developed a demonstrably flexible, computationally  
142 efficient, and robust statistical model that is capable of downscaling any atmospheric variable  
143 that is measured on a daily basis as long as it has, or can be transformed into, an approximately  
144 Gaussian distribution. This approach can be applied globally and to a broad range of climate and  
145 weather data sources, from global and regional model output to satellite data, gridded  
146 observations, and weather station records. Section 2, Model Development, describes the  
147 statistical basis of the model and refinements that improve its ability to downscale global model  
148 outputs. Section 3, Model Performance and Evaluation, describes how the model's ability to  
149 simulate temperature and precipitation extremes across the globe was tested using the perfect  
150 model framework. Finally, Section 4 summarizes the findings of this analysis, its application to  
151 climate impact assessments, and future model development objectives.

152

## 153 2 STAR-ESDM Design and Development

154 STAR-ESDM is a MATLAB-based code that combines signal decomposition with  
155 Fourier filtering and kernel density estimation to create an effective and computationally-  
156 efficient bias-removal and spatial disaggregation technique that can be used to analyze and  
157 translate a coarser-resolution time series of any quasi-Gaussian variable into a finer-resolution  
158 time series of the same variable. It is designed for application to climatological data: specifically,  
159 (1) to analyze biases in GCM and RCM simulations compared to observational or quasi-  
160 observational datasets over timescales relevant to the statistics of climate and weather, and (2) to  
161 use this information to bias-correct and spatially disaggregate predictor projections to the scale  
162 of the input predictands. Predictands can consist of gridded or station-based observations, quasi-  
163 observations such as satellite datasets or reanalysis, or higher resolution model output at any  
164 spatial scale finer than that of the predictor.

165 The first part of the acronym, STAR (seasonal trends and analysis of residuals) refers to  
166 the decomposition of a time series into components based on temporal variability: (1) long-term  
167 decadal average and/or trend, (2) climatological annual cycle (average over the historical period),  
168 (3) dynamical annual cycle (changing over time), and (4) high frequency daily anomalies. The  
169 second part of the acronym, ESDM (empirical-statistical downscaling model) refers to the steps  
170 taken once a modeled predictor and an observed or quasi-observed predictand has been  
171 decomposed into these components. The predictor signal is bias-corrected relative to the  
172 observed or predictand signal for a historical period and the projected changes then applied to  
173 observed values, resulting in bias-corrected and downscaled high-resolution projections at the  
174 spatial scale of the observations.

175 In empirical statistical bias-correction and downscaling, stationarity is a primary concern  
176 (e.g. Dixon et al. 2016). Will statistical relationships developed based on historical data hold true  
177 under potentially very different climatic conditions in the future? In cases where human  
178 intervention directly or indirectly, through climate change, significantly alters the characteristics  
179 of the land surface (e.g. by expanding an urban area, through large-scale deforestation, or when  
180 the timing of snowpack melt shifts), the answer is clearly no. The only way to account for these  
181 in climate modeling, whether statistical or dynamical, is to either explicitly include the change or  
182 build in the capacity to predict the change. In other cases, however, it may be possible to increase  
183 the stationarity of the model by increasing its ability to resolve different components of a signal  
184 that may be changing differently over time: and this is the hypothesis on which STAR-ESDM is  
185 based.

186 Why might signal decomposition improve the stationarity of a statistical model? Biases  
187 and errors in GCM simulations, which arise due to both structural and parametric uncertainties in  
188 the model, are typically physical in origin and relate to a process or a component not accurately  
189 represented in the model for that region or aspect of the climate system. When the GCM signal is  
190 considered in sum, as an 'analogue' signal, it increases the likelihood that some of the biases  
191 interact and even cancel each other out. A statistical method that cannot distinguish between the  
192 various sources of bias must assume that not only the biases, but how they interact with each  
193 other, remain stationary over time. Decomposing the signal by the timescale over which various  
194 types of biases may occur allows them to be better quantified and a statistical correction  
195 developed that is appropriate to the timescale at which they are relevant: effectively 'digitizing'

196 the signal, to a certain extent. Through decomposing the signal, each component of which may  
197 be biased due to different sources of structural or parametric uncertainty within the GCM, these  
198 can be corrected independently before the signal is recombined. Previous evaluations of a beta  
199 version of STAR-ESDM v1 using the perfect model framework (Dixon et al. 2016) shows that  
200 the manner in which it allows distributions of daily anomalies and annual climatology to change  
201 over time relaxes the stationarity assumption that underlies most ESDMs, significantly reducing  
202 the bias, particularly at the tails of the distribution where extreme events may be relatively rare  
203 but have a proportionally greater impact. Based on that preliminary analysis, we have now  
204 developed a fully operational STAR-ESDM v2 can be used to bias-correct and downscale a  
205 broad range of coarser-resolution predictor datasets to finer-resolution predictands, and evaluate  
206 its stationarity here.

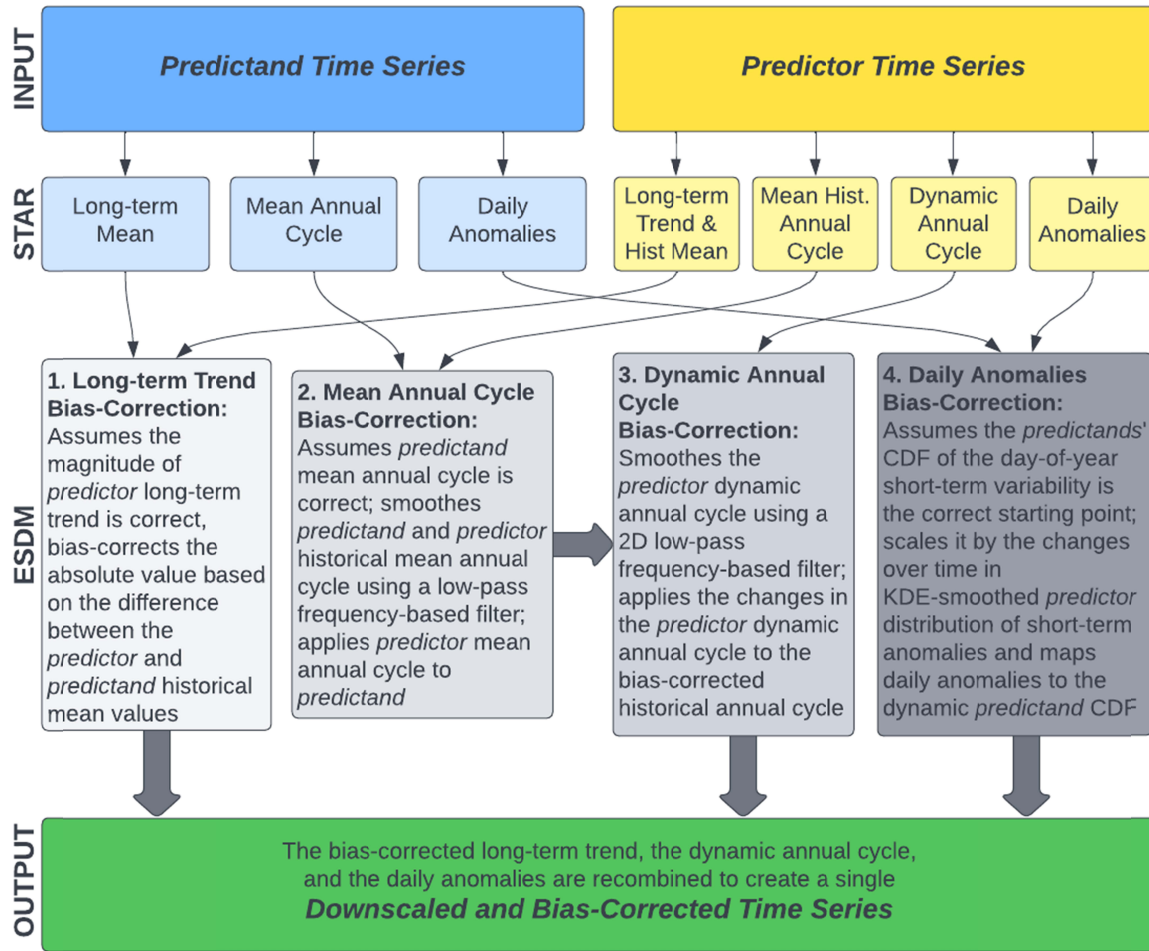
207 Applying the STAR-ESDM framework to bias-correct and spatially disaggregate coarser  
208 predictor simulations (which could be derived from any dataset a user wishes to bias-correct and  
209 downscale, but are most likely to consist of GCM or RCM output) relative to a higher-resolution  
210 predictand dataset consists of three main steps (Figure 1). First, each time series is disaggregated  
211 into individual components. Second, predictand components are used to bias-correct predictor  
212 components, and predictor components are used to map predictand statistics to future conditions.  
213 Lastly, bias-corrected and downscaled components are recombined to create a single continuous  
214 time series at the spatial scale of the predictand but covering the temporal range of the predictor.

215 The first component is the long-term trend, determined by fitting an optimized linear or  
216 third-order trend to the entire time series. This represents the climatological change resulting  
217 from human choices. Based on analyses comparing model-simulated with observed multi-  
218 decadal trends at the regional to global scale (IPCC, 2021a), the framework currently assumes  
219 that the absolute value of the predictand and the long-term normalized trend of the predictor are  
220 accurate.

221 The second component is the mean or climatological annual cycle over the historical  
222 period. It is extracted by averaging each day of the year over the historical period, then  
223 smoothing the resulting curve using a low-pass Fourier filter to remove noise. This was used in  
224 place of a conventional smoothing filter such as a rolling mean to prevent dampening the  
225 extremes. The historical period is flexible, automatically determined based on the beginning and  
226 end of the predictand data being used. Thus, if a longer dataset or a more recently updated one is  
227 being used, predictand values beginning as far back as 1900 or ending as recently as the latest  
228 full year of predictand data will be considered part of the historical “training” period; whereas if  
229 a relatively short predictand dataset such as 1971-2000 is being used, then only this period will  
230 be used to determine the static annual cycle as well as the components that follow. The  
231 difference between the predictand and predictor annual cycle is used to bias-correct the  
232 predictor’s dynamic annual cycle (how it varies from year to year).

233 The third component is the annually-varying or dynamical annual cycle. This component  
234 is smoothed both along the year axis and the day-of-year axis to create a climatological surface  
235 that changes over time, but with the variability and the long-term trend over both day to day and  
236 year to year timescales removed. This is then used to adjust the predictand annual cycle to  
237 account for future changes. It captures the change in the shape of the climatology over time,  
238 accounting for how summer may be broadening, for example, and shoulder seasons shrinking, or

239 how the timing of the monsoon season may be shifting, independent of long-term trends in  
 240 average annual values or short-term daily variability. Changes in the predictor-simulated annual  
 241 cycle over time are then used to extend the predictand climatology into the future.



242

243 **Figure 1.** The STAR-ESDM framework decomposes the predictor (model) and predictand  
 244 (observed or quasi-observed) time series into components which are then used to individually  
 245 bias-correct predictor and/or adjust predictand components as shown here. Components are then  
 246 recombined to generate a continuous high resolution time series of climate projections at the  
 247 spatial scale of, and matching the statistical properties of, the predictand dataset but covering the  
 248 time period of the predictor dataset.

249 To correct biases in and downscale projected changes in the annual cycle, we make the  
 250 following assumptions which allow for relaxation of certain stationarity assumptions. First, we  
 251 assume that while the shape of the predictor's annual cycle most likely contains biases, predicted  
 252 changes in the shape of the annual cycle are a reasonable approximation to how the predictand's  
 253 climatology would change over time, given the assumptions underlying the predictor and its  
 254 inputs. Similarly, we assume that the changes over time to the shape of the predictor's daily  
 255 probability distributions, described as cumulative distribution functions (CDFs), are a reasonable

256 estimate of the likely changes in the predictand's CDFs over time as well. The former allows the  
257 bias-corrected annual signal to vary over time, and the latter allows mapping of the predictor's  
258 daily anomalies from the predictor's time-varying CDFs to an estimate of the predictand's time-  
259 varying CDFs, rather than to a static historical CDF.

260 Another important feature of STAR-ESDM is that creates probability surfaces of the  
261 annual cycles rather than discrete monthly CDFs. These surfaces are generated for both the  
262 historical period and future conditions using a rolling window that steps forward through time.  
263 Two-dimensional frequency-based (Fourier domain) filtering of the probability surfaces ensures  
264 they vary smoothly, with unique values for each day of the year. Similarly, one-dimensional  
265 Fourier filtering is used to smooth the static or climatological annual cycles for the predictand's  
266 and the predictor's historical period data, and two-dimensional filtering is used to calculate  
267 dynamic annual cycle surfaces which evolve over time by combining the observations' historical  
268 and model future data. Thus, the dynamic annual cycle surface represents the expected value of  
269 the data variable over time, while the probability surfaces represents the variability of the data  
270 variable, both in the historical period and over time. The predictor's annual cycle is adjusted to  
271 match the mean value and shape of the predictand's in the historical period, and allowed to vary  
272 over time as estimated by the predictor through the full time period from past into the future.

273 The frequency range of the filters is selected to allow separating the signal into the  
274 seasonally varying component (climatology) and the short-term variability (weather).  
275 Seasonally-varying filters capture 90 to 95 percent of typical seasonal-shape changes, including  
276 events that repeat annually but excluding short-term random events. Once these three  
277 components have been removed from the signal, what remains primarily reflects high-frequency  
278 daily variability in the time series which may not repeat from year to year. This last component  
279 characterizes the magnitude and frequency of extremes, which are the most challenging aspect of  
280 future projections for ESDMs to accurately resolve, and simultaneously the most relevant to  
281 many stakeholder applications in building climate resilience to threats including heatwaves,  
282 droughts, floods and more.

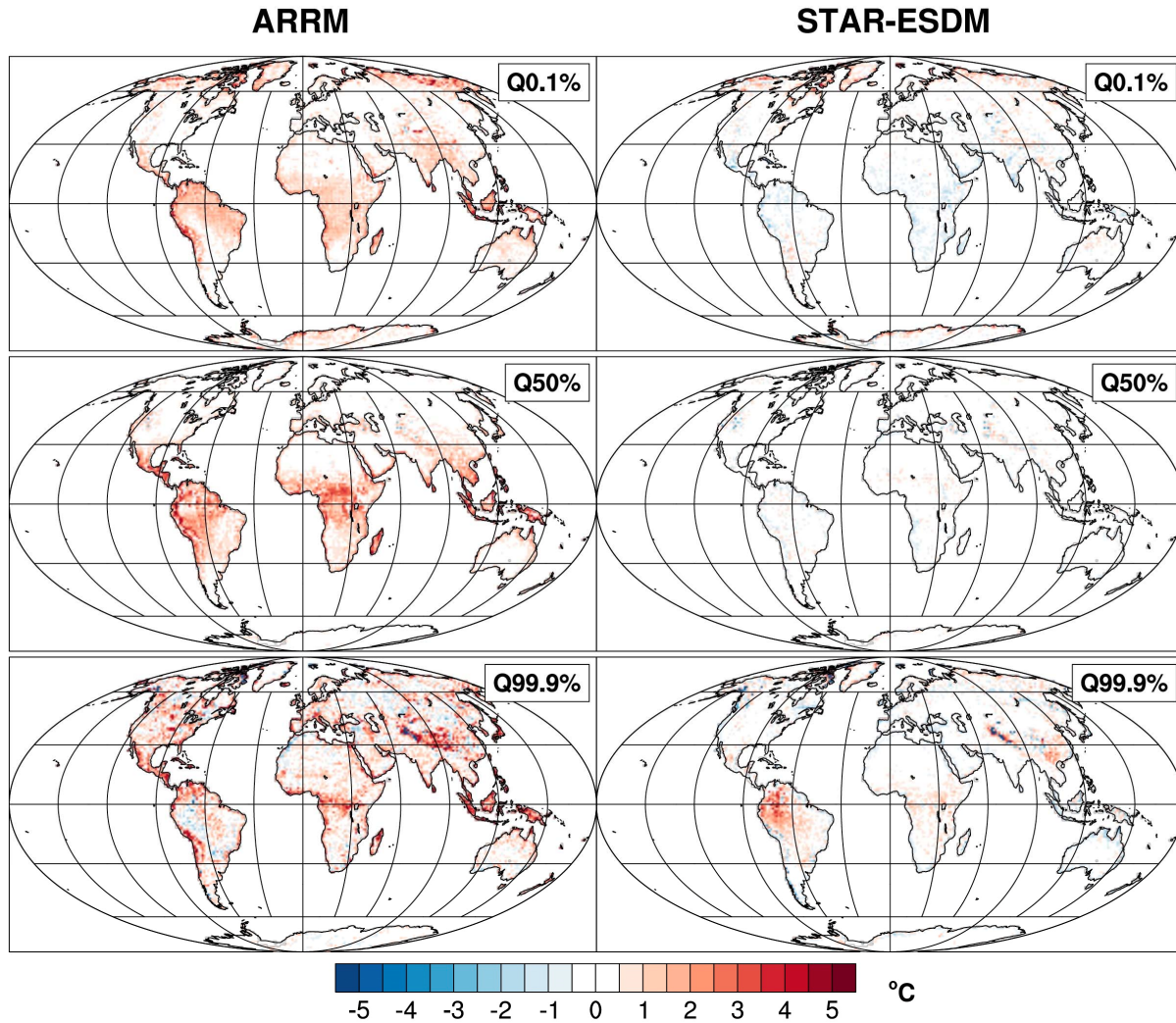
283 Daily anomaly values are bias-corrected by calculating a quantile value for each data  
284 point and mapping between the predictor's set of rolling CDFs and the predictand's set of rolling  
285 estimated CDFs. Filtering of daily variability is also done in the Fourier domain as it is much  
286 faster computationally than using time-domain convolution, and computational efficiency is  
287 another key consideration in development of this model. Finally, one last round of Fourier  
288 filtering combined with Kernel Density Estimation (KDE) smoothing is used to transform the  
289 two-dimensional histograms of the anomalies into PDF surfaces, which are then integrated along  
290 the probability axis to create CDF surfaces; KDE being an approach determined by McGinnis et  
291 al. (2015) to perform well in bias correcting climate model output.

292 These steps are generalizable to any variable with a quasi-Gaussian distribution or that  
293 can be transformed into a quasi-Gaussian form. As discussed in the next section, however,  
294 through iterative application of the Perfect Model framework, the method has been optimized to  
295 daily maximum and minimum temperature and precipitation (and in the future, will be similarly  
296 optimized to apply the model to humidity, solar radiation, and more).

### 297 **3 Model Performance and Evaluation**

298 We evaluate the stationarity of the STAR-ESDM framework using a “Perfect Model”  
299 framework. As described in Dixon et al. (2016), the name of this approach is not intended to  
300 contradict the aphorism often attributed to statistician George Box, “All models are wrong but  
301 some are useful.” Rather, “Perfect Model” describes a methodology that uses a high-resolution  
302 GCM simulation (in this case, a 25km resolution GFDL simulation for a historical period and for  
303 an end-of-century 2086-2095 RCP8.5 scenario) and a coarsened version of the same simulation  
304 as the predictand and predictor variables to train an ESDM in a “pseudo-reality context,” as  
305 Erlandsen et al. (2020) describe it. The resulting ESDM is then applied to the coarsened GCM  
306 simulations in the future and the output compared to the fully dynamical simulations for the  
307 same time period. Differences between the statistically bias-corrected and downscaled ESDM  
308 and dynamical GCM output for the same future time period reveal structural uncertainties in the  
309 ESDM that prevent it from generating the information that a much more complex (but less  
310 flexible and more computationally demanding) dynamical high-resolution global climate model  
311 would. Locations where biases are minimal indicate that the ESDM can generate virtually  
312 identical values to those of a fully dynamical model (with the benefits of greater flexibility and  
313 significantly reduced computational cost, as well as bias-correction).

314 To illustrate the improvement offered by the signal processing approach, we compare the  
315 biases in STAR-ESDM output with the biases in projections generated using the Asynchronous  
316 Regional Regression Model, a parametric quantile mapping approach to bias correction and  
317 downscaling that has been used in a number of regional climate assessments across the United  
318 States (Stoner et al. 2012). As shown in Figure 2, while ARRM performed well over the  
319 contiguous United States at simulating daily maximum temperature for quantiles ranging  
320 between 0.1 and 99.9, it displayed biases in maximum temperature values ranging from 3 to 5°C  
321 for both extreme hot and cold temperatures along most major coastlines and biases in mean  
322 values averaging around 3°C across much of Central and South America and central Africa that  
323 would preclude its use in those regions. In contrast, STAR-ESDM displays almost no biases in  
324 mean values across any continental area other than a bias of between 1-2°C at the highest  
325 elevations of the Rocky and Himalayan mountain ranges. Even out to the tails of the distribution,  
326 at the 0.1 and 99.9th quantiles, biases are significantly reduced in both extent and magnitude  
327 relative to ARRM. For the 1-in-1000 coldest temperatures, STAR-ESDM warm biases occur  
328 primarily along Arctic coastlines, while for the 1-in-1000 highest temperatures, significant warm  
329 and cold biases are present only in the northern Andes and the highest elevation region of the  
330 Himalayas. Table S1 summarizes the locations where STAR-ESDM use is not recommended for  
331 temperature projections, and Figure S2 shows the same results as in Figure 1, except for daily  
332 minimum temperature.

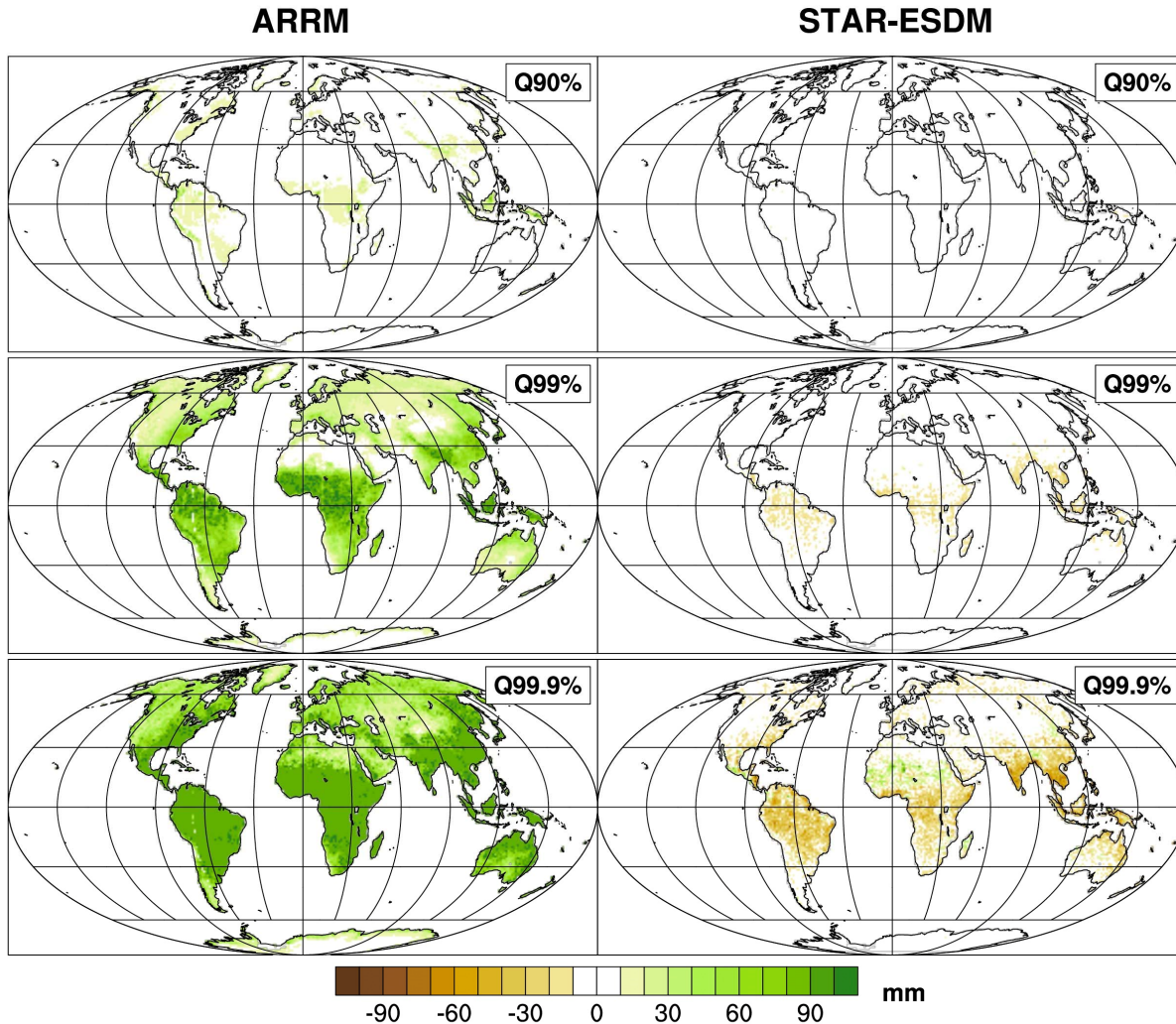


333

334 **Figure 2.** Biases over land areas in ARRМ (left) and STAR-ESDM (right) daily maximum  
 335 temperature (degrees C) compared to high resolution global climate model output for 2086-2095  
 336 under the higher RCP8.5 scenario for the 1-in-1000 coldest, mean, and 1-in-1000 hottest days  
 337 illustrate the significant improvements the signal processing approach uses over the parametric  
 338 quantile mapping approach.

339 Improvements in precipitation are even more pronounced. (Here, precipitation quantiles  
 340 are calculated based on wet days only. As such, they represent a more extreme assessment than  
 341 temperature quantiles, which are calculated based on all days.) As shown in Figure 3, ARRМ is  
 342 capable of simulating projected changes in precipitation over the contiguous United States,  
 343 northern Africa, the Middle East, and Europe up to the 90th quantile of wet day precipitation  
 344 with minimal biases. Biases of 20-30 mm/day occurred over South America, central Africa, and  
 345 southeast Asia. At the 99th quantile, however, positive biases ranging from 20 to 40 mm per day  
 346 across the contiguous United States and up to 100mm per day across other continental areas  
 347 occurred. By the 99.9th quantile, positive biases ranging from 50 up to greater than 100mm per  
 348 day occurred across most continental areas. STAR-ESDM biases are less than 10 mm per day at  
 349 the 90th quantile across all land areas. At the 99th quantile, small negative biases on the order of

350 10 to 20 mm per day occur across equatorial regions (within about 10 degrees of the equator)  
 351 while biases across the rest of the world remain below 10 mm per day. At the 99.9th quantile,  
 352 while negative biases approaching 50 mm emerge in equatorial regions, biases across most of  
 353 North America, Europe, and central Asia remain below 10 mm. This indicates that even for the  
 354 wettest few days in a decade, the statistical model is able to reproduce the values that a high-  
 355 resolution dynamical model would provide at that quantile. Once again, Table S1 summarizes  
 356 the locations, quantiles and seasons where STAR-ESDM use is not recommended for  
 357 precipitation.

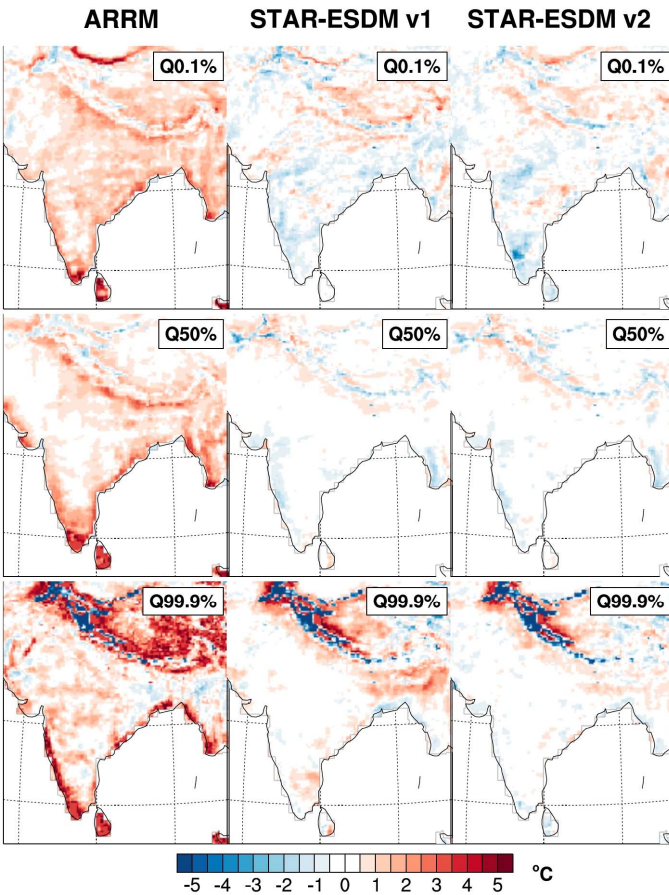


358

359 **Figure 3.** Biases over land areas in ARRM (left) and STAR-ESDM (right) daily cumulative  
 360 precipitation values (mm per day) compared to 25km global climate model output for 2086-2095  
 361 under the higher RCP8.5 scenario for the 1-in-10, 1-in-100, and 1-in-1000 wettest days of all wet  
 362 days at that location illustrate the stationarity of the STAR approach and the significant  
 363 improvements the signal processing approach uses over the parametric quantile mapping  
 364 approach.

365 As discussed in the section above, the signal processing approach used by STAR-ESDM  
 366 already offers significant improvements relative to previous statistical methods. However, a

367 second unique aspect of this work is that STAR-ESDM was not developed linearly. Rather, we  
 368 used the Perfect Model framework to iteratively and interactively optimize the original code for  
 369 daily maximum and minimum temperature and 24-hour cumulative precipitation. This enabled  
 370 us to identify areas with high biases, and explore statistical approaches to reducing those biases  
 371 that were: (a) consistent with the likely physical basis of the bias, and (b) globally generalizable,  
 372 to avoid over-fitting.



373

374 **Figure 4.** Biases in ARRМ (left), STAR-ESDM v1 (center) and STAR-ESDM v2 (right) daily  
 375 maximum temperature (degrees C) compared to high resolution global climate model output for  
 376 2086-2095 under the higher RCP8.5 scenario for the 0.1, 50th and 99.9th quantiles of the  
 377 distribution over the Indian subcontinent show how both the statistical method and the further  
 378 refinement using the Perfect Model approach reduce biases compared with previous methods.

379

380 When comparing STAR-ESDM v1 (the original generic code) with v2 (the code that has  
 381 been iteratively optimized) at the global scale, there are few obvious improvements in maximum  
 382 and minimum temperature biases, other than a reduction in the magnitude of high quantile biases  
 383 in equatorial regions (Figures S1 and S2). At a finer scale, however, the added value of these  
 384 refinements can be more evident. In high-elevation locations, for example, shifts in the timing of  
 385 snow melt lead to large positive and negative temperature biases in spring and summer. Figure 4  
 386 compares biases in maximum temperature projections over the Indian subcontinent

387 corresponding to ARRM, STAR-ESDM v1 and STAR-ESDM v2. While the greatest  
388 improvements are still obtained by changing the statistical approach, at the 99.9th quantile it can  
389 be seen that an outlier adjustment that was part of the original v1 design (scaling daily extremes  
390 beyond 2.5 sigma) produced slightly greater biases than simply smoothing the entire time series  
391 using the KDE. Removing this scaling further reduced the bias at mid elevations and in the  
392 foothills and expanded the geographic area over which this method can effectively be used in v2.

393 Precipitation is a more challenging variable to characterize than temperature and as a  
394 result, for this variable the Perfect Model optimization yielded greater benefits. As shown in  
395 Figure S4, STAR-ESDM v1 output for the 99th and 99.9th quantile was characterized by large  
396 bands of positive and negative precipitation biases across equatorial regions, while continental  
397 biases were less but still notable, ranging from -20 mm per day across the Gulf Coast up to 50  
398 mm per day at high elevations in the Andes and Himalayas. We first explored the use of different  
399 methods to transform precipitation into an approximately Gaussian distribution, and identified  
400 power mapping as the most consistent. However, originally v1 used the same empirically-  
401 determined power mapping for all locations. Adding an iterative search to identify the optimal  
402 equation for each individual location reduced precipitation biases in equatorial regions in terms  
403 of both geographic extent and magnitude, while biases across continental areas in the northern  
404 hemisphere were reduced to less than +/- 5 mm per day. While a dry bias persists across South  
405 America, southern Africa and southeast Asia in v2, the magnitude of the bias ranges from -5 to -  
406 15 mm per day, nearly an order of magnitude reduction compared to STAR-ESDM v1.

407 As alluded to earlier, quantifying biases using the Perfect Model approach also enables us  
408 to identify geographic locations where use of this framework is not recommended as the ESDM  
409 displays significant non-stationarity; these locations and quantiles are listed in Table S1. For  
410 example, shifts in the timing of monsoonal precipitation in a warmer world may be what leads to  
411 precipitation biases across Central America, Mexico and the southwestern United States that  
412 dominate during spring and summer seasons. Similarly, large biases in temperature values still  
413 occur under a set of specific conditions, including biases (a) in high temperatures for very high  
414 elevations in the Andes and Himalayas under a higher scenario by end of century, during the  
415 season that saw the highest level of snow melt during the historical period, and (b) in both high  
416 and low temperatures along Arctic coastlines where rapid melting of shoulder-season sea ice  
417 introduces significant non-stationarity relative to historical conditions. In these cases, the biases  
418 are likely due to the fact that the statistical relationships between predictor and predictand for  
419 future months are now representative of those of a different month in the historical time period.  
420 In future versions of STAR-ESDM, this can be addressed by introducing a phase shift into the  
421 bias corrections applied to the dynamical climatology and the high frequency variability.  
422 Effective reduction of other biases might require more granular information that is absent in the  
423 coarser-scale model, such as distinguishing between land and air temperatures for small islands  
424 below the spatial scale of the predictor grid cell, or for valleys and mountains in areas with  
425 rapidly-varying topography. In the future, we plan to explore whether these could be improved  
426 through incorporating high-resolution digital elevation maps, lapse rates, and more into the  
427 statistical model.

#### 428 **4 Conclusions and Next Steps**

429 As anthropogenic climate change increasingly impacts food production, water quality,  
430 infrastructure integrity, and the frequency and intensity of extreme events, there is a critical need

431 for accurate and high-resolution climate projections to inform sectoral and regional climate  
432 resilience planning. The STAR-ESDM model, developed within the Perfect Model framework,  
433 represents a significant advancement in the ability to generate robust high-resolution climate  
434 projections for regional to local-scale climate impact assessments. As described above, the  
435 STAR-ESDM model decomposes a predictand and predictor signal into multiple components  
436 which are then bias-corrected and adjusted individually before being recombined into a single  
437 coherent time series covering the time period of the predictor. The result is a stationary and  
438 computationally-efficient ESDM which was further iteratively developed within the Perfect  
439 Model framework to quantify model biases by variable, region and season. Additionally, it is  
440 extremely flexible, allowing for a range of predictor and predictand inputs, depending on what is  
441 available for that region.

442 Evaluating STAR-ESDM's ability to bias correct and downscale climate projections for  
443 end-of-century under a higher (RCP8.5) scenario by comparing its output to that of a high-  
444 resolution dynamical model demonstrates that, for quantiles ranging from 0.1 to 99.9 over most  
445 land areas, it is able to produce temperature and precipitation projections that are virtually  
446 identical to those that would be obtained from a high-resolution fully dynamical model. With a  
447 few exceptions, such as the Arctic coastline and areas with rapidly varying topography at high  
448 elevation such as the Himalayas, STAR-ESDM can be confidently applied to nearly any location  
449 in the world for which gridded or point-based predictand data is available. The granularity of this  
450 guidance, as summarized in Table S1, offers stakeholders and users a clear pathway to assessing  
451 the reliability of this information for informing their future assessments, depending on which  
452 quantiles of the distribution, geographic location, and season(s) are most relevant to the impacts  
453 with which they are concerned.

454 We have already applied the STAR-ESDM framework to generating high-resolution  
455 projections of daily maximum and minimum temperature and precipitation using SSP1-2.6,  
456 SSP2-4.5, SSP3-7.0, and SSP5-8.5 simulations by 24 CMIP6 GCMs as predictors for the  
457 following geographic regions and predictand datasets: (1) the contiguous U.S. using the  
458 NCLimGrid 5x5km observational dataset (Vose et al. 2014), (2) the contiguous U.S. using to the  
459 Livneh 1/16th degree observational dataset (Livneh et al. 2015), and (3) North and Central  
460 America and the Caribbean, using over 10,000 GHCNd long-term weather station records  
461 (Menne et al. 2012). We are currently extending this work to the global scale, using Sheffield et  
462 al. (2006) global 0.25 x 0.25 degree gridded dataset and the ERA5-Land 0.1 x 0.1 degree global  
463 dataset (Muñoz-Sabater et al., 2021) as predictands to generate global high-resolution bias-  
464 corrected projections. These datasets will be archived shortly; we anticipate we will be able to  
465 remove this sentence and include a DOI for each of these datasets by the time this manuscript is  
466 published.

467 In future model development, we propose to examine projected phase shifts in annual  
468 cycles to determine whether it is possible to reduce biases arising from to changes in the timing  
469 of monsoonal precipitation or snowpack melt at high elevations. We also plan to refine the  
470 weighting scheme used to select predictor grid cells, to better characterize conditions in areas of  
471 rapidly varying topography such as islands, coastlines, and mountainous areas, and explore the  
472 outcomes of including a high resolution digital elevation map. Finally, recognizing that a  
473 fundamental flaw in statistical methods is the separation and independent bias-correction of  
474 variables that are dynamically linked, long-term we propose to develop a version of STAR-

475 ESDM where the input is a hypersurface composed of average temperature, daily temperature  
476 range, humidity and precipitation, rather than a single variable.

477         As the need for accurate and detailed climate impact assessments increases, high-  
478 resolution climate projections will play a crucial role in helping societies worldwide adapt to and  
479 mitigate the impacts of climate change. STAR-ESDM provides a valuable tool for resilience and  
480 adaptation planning, especially in the most vulnerable regions which often lack abundant  
481 observational data or modeling capacity.

482

### 483 **Acknowledgments**

484 We thank Keith Dixon and John Lanzante for many fruitful discussions that greatly informed the  
485 direction of this work. In addition to their positions listed here, K. Hayhoe is the owner of  
486 ATMOS Research, a non-publicly traded entity and both K. Hayhoe and A. Stoner have served  
487 as consultants in developing and contributing to various regional climate assessments and  
488 climate action plans. K. Hayhoe, I. Scott-Fleming and A. Stoner were supported by Texas Tech  
489 University and A. Stoner and D. Wuebbles by Earth Knowledge in the development of this work.

490

### 491 **Open Research**

492 Version 2.0 of the STAR-ESDM MATLAB code, the development and evaluation of which is described in this  
493 manuscript, will be made freely available for download via a Github public repository prior to publication. A  
494 permanent link to the code repository and a DOI will be provided with article revisions.

495

### 496 **References**

497 Barsugli, J., G. Guentchev, R. M. Horton, A. Wood, L. O. Mearns, X.-L. Liang, J. Winkler, K.  
498 Dixon, K. Hayhoe, R. B. Rood, L. Goddard, A. Ray, L. Buja & C. Ammann (2013), The  
499 Practitioner's Dilemma: How to Assess the Credibility of Downscaled Climate Projections. *EOS*,  
500 *94*(46), 424-425, doi:10.1002/2013EO460005

501

502 Chen, D., M. Rojas, B.H. Samset, K. Cobb, A. Diongue Niang, P. Edwards, S. Emori, S.H. Faria,  
503 E. Hawkins, P. Hope, P. Huybrechts, M. Meinshausen, S.K. Mustafa, G.-K. Plattner, & A.-M.  
504 Tréguier (2021) Framing, Context, and Methods. In *Climate Change 2021: The Physical Science*  
505 *Basis. Contribution of Working Group I to the Sixth Assessment Report of the Intergovernmental*  
506 *Panel on Climate Change* [Masson-Delmotte, V., P. Zhai, A. Pirani, S.L. Connors, C. Péan, S.  
507 Berger, N. Caud, Y. Chen, L. Goldfarb, M.I. Gomis, M. Huang, K. Leitzell, E. Lonnoy, J.B.R.  
508 Matthews, T.K. Maycock, T. Waterfield, O. Yelekçi, R. Yu, and B. Zhou (eds.)]. Cambridge  
509 University Press, Cambridge, United Kingdom and New York, NY, USA, pp. 147–286,  
510 doi:10.1017/9781009157896.003.

511

512 Coulibaly, P., Y. Dibike & F. Anctil (2005), Downscaling Precipitation and Temperature with  
513 Temporal Neural Networks. *Journal of Hydrometeorology*, 6(4), 483-496,  
514 doi:10.1175/JHM409.1

515

516 Dixon, K., J. Lanzante, M.J. Nath, K. Hayhoe, A. Stoner, A. Radhakrishnan, V. Balaji & C.  
517 Gaitán (2016), Evaluating the stationarity assumption in statistically downscaled climate  
518 projections: is past performance an indicator of future results? *Climatic Change*, 135(3-4), 395-  
519 408, doi:10.1007/s10584-016-1598-0

520

521 Erlandsen, H., K. Parding, R. Benestad, A. Mezghani & M. Pontoppidan (2020), A hybrid  
522 downscaling approach for future temperature and precipitation change. *Journal of Applied*  
523 *Meteorology and Climatology*, 59(11), 1793-1807, doi: 10.1175/JAMC-D-20-0013.1

524

525 Glahn, H. & D. Lowry (1972), The use of Model Output Statistics (MOS) in objective weather  
526 forecasting. *Journal of Applied Meteorology and Climatology*, 11(8), 1203-1211,  
527 doi:10.1175/1520-0450(1972)011%3C1203:TUOMOS%3E2.0.CO;2

528

529 Hayhoe, K., D. Cayan, C. B. Field, P. C. Frumhoff, E. P. Maurer, N. L. Miller, S. C. Moser, S.  
530 H. Schneider, K. Nicholas, E. E. Cleland, L. Dale, R. Drapek, R. M. Hanemann, L. S. Kalkstein,  
531 J. Lenihan, C. K. Lunch, R. P. Neilson, S. C. Sheridan, & J. H. Verville (2004), Emissions  
532 pathways, climate change, and impacts on California. *Proceedings of the National Academy of*  
533 *Sciences*, 101(34), 12422-12427, doi:10.1073/pnas.0404500101

534

535 Hayhoe, K., C. Wake, B. Anderson, X-Z Liang, E. Maurer, J. Zhu, J. Bradbury, A. DeGaetano,  
536 A. Stoner & D. Wuebbles (2007), Regional climate change projections for the Northeast USA.  
537 *Mitigation and Adaptation Strategies for Global Change*, 13, 425-436, doi:10.1007/s11027-007-  
538 9133-2

539

540 Hayhoe, K., J. Edmonds, R.E. Kopp, A.N. LeGrande, B.M. Sanderson, M.F. Wehner, & D.J.  
541 Wuebbles (2017), Climate models, scenarios, and projections. In: *Climate Science Special*  
542 *Report: Fourth National Climate Assessment, Volume I* [Wuebbles, D.J., D.W. Fahey, K.A.  
543 Hibbard, D.J. Dokken, B.C. Stewart, and T.K. Maycock (eds.)]. U.S. Global Change Research  
544 Program, Washington, DC, USA, pp. 133-160, doi:10.7930/J0WH2N54.

545

546 Hayhoe, K., I. Scott-Fleming, A. Stoner and D. Wuebbles, (2023), STAR-ESDM Version 2.0  
547 [Software], Github repository link and DOI TBD.

548

549 Hernanz, A. J. A. Garcia-Valero, M. Dominguez & E. Rodriguez-Camino (2022), A critical view  
550 on the suitability of machine learning techniques to downscale climate change projections:  
551 Illustration for temperature with a toy experiment. *Atmospheric Science Letters*, 23(6), e1087,  
552 doi:10.1002/asl.1087

553

554 IPCC (2021a), Summary for Policymakers. In: *Climate Change 2021: The Physical Science*  
555 *Basis. Contribution of Working Group I to the Sixth Assessment Report of the Intergovernmental*  
556 *Panel on Climate Change* [Masson-Delmotte, V., P. Zhai, A. Pirani, S.L. Connors, C. Péan, S.  
557 Berger, N. Caud, Y. Chen, L. Goldfarb, M.I. Gomis, M. Huang, K. Leitzell, E. Lonnoy, J.B.R.  
558 Matthews, T.K. Maycock, T. Waterfield, O. Yelekçi, R. Yu, and B. Zhou (eds.)]. Cambridge  
559 University Press, Cambridge, United Kingdom and New York, NY, USA

560

561 IPCC (2021b), Annex II: Models [Gutiérrez, J M., A.-M. Tréguier (eds.)]. In: *Climate Change*  
562 *2021: The Physical Science Basis. Contribution of Working Group I to the Sixth Assessment*  
563 *Report of the Intergovernmental Panel on Climate Change* [Masson-Delmotte, V., P. Zhai, A.  
564 Pirani, S.L. Connors, C. Péan, S. Berger, N. Caud, Y. Chen, L. Goldfarb, M.I. Gomis, M. Huang,  
565 K. Leitzell, E. Lonnoy, J.B.R. Matthews, T.K. Maycock, T. Waterfield, O. Yelekçi, R. Yu, and  
566 B. Zhou (eds.)]. Cambridge University Press, Cambridge, United Kingdom and New York, NY,  
567 USA, pp. 2087–2138, doi:10.1017/9781009157896.016.

568

569 IPCC (2022), Summary for Policymakers [H.-O. Pörtner, D.C. Roberts, E.S. Poloczanska, K.  
570 Mintenbeck, M. Tignor, A. Alegría, M. Craig, S. Langsdorf, S. Löschke, V. Möller, A. Okem  
571 (eds.)]. In: *Climate Change 2022: Impacts, Adaptation and Vulnerability. Contribution of*  
572 *Working Group II to the Sixth Assessment Report of the Intergovernmental Panel on Climate*  
573 *Change* [H.-O. Pörtner, D.C. Roberts, M. Tignor, E.S. Poloczanska, K. Mintenbeck, A. Alegría,  
574 M. Craig, S. Langsdorf, S. Löschke, V. Möller, A. Okem, B. Rama (eds.)]. Cambridge  
575 University Press, Cambridge, UK and New York, NY, USA, 3–33,  
576 doi:10.1017/9781009325844.001.

577

578 Karl, T., W-C Wang, M. Schlesinger, R. Knight & D. Portman (1990), A Method of Relating  
579 General Circulation Model Simulated Climate to the Observed Local Climate. Part I: Seasonal  
580 Statistics. *Journal of Climate*, 3(10), 1053-1079, doi:10.1175/1520-  
581 0442(1990)003%3C1053:AMORGC%3E2.0.CO;2

582

583 Kotamarthi, R., K. Hayhoe, L. Mearns, D. Wuebbles, J. Jacobs & J. Jurado (2021), *Downscaling*  
584 *Techniques for High-Resolution Climate Projections: From Global Change to Local Impacts*.  
585 Cambridge University Press, doi:10.1017/9781108601269

586

587 Livneh, B., Bohn, T., Pierce, D. et al. (2015). A spatially comprehensive, hydrometeorological  
588 data set for Mexico, the U.S., and Southern Canada 1950–2013. *Sci Data*, 2, 150042,  
589 doi:10.1038/sdata.2015.42

590

591 McGinnis, S., D. Nychka & L. O. Mearns (2015), A New Distribution Mapping Technique for  
592 Climate Model Bias Correction. In: Lakshmanan, V., Gilleland, E., McGovern, A., Tingley, M.  
593 (eds) *Machine Learning and Data Mining Approaches to Climate Science*. Springer, Cham.  
594 doi:10.1007/978-3-319-17220-0\_9  
595

596 Menne, M.J., I. Durre, R.S. Vose, B.E. Gleason, & T.G. Houston (2012), An overview of the  
597 Global Historical Climatology Network-Daily Database. *Journal of Atmospheric and Ocean*  
598 *Technology*, 29, 897-910, doi:10.1175/JTECH-D-11-00103.1.  
599

600 Muñoz-Sabater, J., Dutra, E., Agustí-Panareda, A., Albergel, C., Arduini, G., Balsamo, G.,  
601 Boussetta, S., Choulga, M., Harrigan, S., Hersbach, H., Martens, B., Miralles, D. G., Piles, M.,  
602 Rodríguez-Fernández, N. J., Zsoter, E., Buontempo, C., & Thépaut, J.-N. (2022), ERA5-Land: A  
603 state-of-the-art global reanalysis dataset for land applications, *Earth Syst. Sci. Data*, 13, 4349–  
604 4383, 2021, doi:10.5194/essd-13-4349-2021.  
605

606 Sachindra, D., K. Ahmed, M. M. Rashid, S. Shahid & B. Perera (2018), Statistical downscaling  
607 of precipitation using machine learning techniques. *Atmospheric Research*, 212, 240-258,  
608 doi:10.1016/j.atmosres.2018.05.022  
609

610 Sheffield, J., G. Goteti & E. Wood (2006), Development of a 50-Year High-Resolution Global  
611 Dataset of Meteorological Forcings for Land Surface Modeling. *Journal of Climate*, 19(13),  
612 3088-3111, doi:10.1175/JCLI3790.1  
613

614 Vose, Russell S., Applequist, S., Squires, M., Durre, I., Menne, M. J., Williams, C. N. Jr.,  
615 Fenimore, C., Gleason, K, and Arndt, D. (2014), *NOAA Monthly U.S. Climate Gridded Dataset*  
616 (*NClimGrid*), *Version 1*. NOAA National Centers for Environmental Information,  
617 doi:10.7289/V5SX6B56 [Jan 2023].

618

619 Vrac, M., M. Stein & K. Hayhoe (2007a), Statistical downscaling of precipitation through  
620 nonhomogeneous stochastic weather typing. *Climate Research*, 34(3), 169-184,  
621 doi:10.3354/cr00696

622

623 Vrac, M., M. L. Stein, K. Hayhoe & X.-Z. Liang (2007b), A general method for validating  
624 statistical downscaling methods under future climate change. *Geophysical Research Letters*,  
625 34(18), doi:10.1029/2007GL030295

626

627 Walton, D., F. Sun, A. Hall & S. Capps (2015), A Hybrid Dynamical–Statistical Downscaling  
628 Technique. Part I: Development and Validation of the Technique. *Journal of Climate*, 28(12),  
629 4597-4617, doi:10.1175/JCLI-D-14-00196.1

630

631 Wang, F. & D. Tian (2022), On deep learning-based bias correction and downscaling of multiple  
632 climate models simulations. *Climate Dynamics*, 59, 3451-3468, doi:10.1007/s00382-022-06277-

633 2

634

635 Wilby, R., C. Dawson & E. Barrow (2002). SDSM – a decision support tool for the assessment  
636 of regional climate change impacts. *Environmental Modelling & Software*, 17(2), 145-157, doi:  
637 10.1016/S1364-8152(01)00060-3

638